

A quantitative analysis of Gravitational Wave spectrum sourced from First-Order Chiral Phase Transition of QCD

Hui-wen Zheng,^{1,*} Fei Gao,^{2,†} Ligong Bian,^{3,4,‡} Si-xue Qin,^{3,§} and Yu-xin Liu^{1,4,5,¶}

¹*Department of Physics and State Key Laboratory of Nuclear Physics and Technology, Peking University, Beijing 100871, China.*

²*School of Physics, Beijing Institute of Technology, 100081 Beijing, China*

³*Department of Physics and Chongqing Key Laboratory for Strongly Coupled Physics, Chongqing University, Chongqing 401331, China.*

⁴*Center for High Energy Physics, Peking University, Beijing 100871, China.*

⁵*Collaborative Innovation Center of Quantum Matter, Beijing 100871, China.*

(Dated: February 12, 2025)

We investigate the cosmological first-order chiral phase transition of QCD, and for the first time calculate its parameters which can determine the gravitational wave spectrum. With the state-of-the-art calculation from the functional QCD method, we found that the large chemical potential of QCD phase transition results in very weak and fast first-order phase transitions at the temperature lower than $\mathcal{O}(10^2)$ MeV. These results further suggest that the GW signals of NANOGrav are very unlikely sourced from the chiral phase transition of QCD.

Keywords: gravitational waves, cosmic QCD transition, lepton asymmetry, functional QCD

Introduction. The space-based interferometers, such as μ Ares [1], Taiji [2, 3], Tianqin [4, 5], the Laser Interferometer Space Antenna (LISA) [6–9], the Big Bang Observer (BBO) [10, 11] and the Deci-Hertz Interferometer Gravitational Wave Observatory (DECIGO) [12–14], offer a frequency window from 10^{-7} Hz to 10 Hz for detecting the stochastic gravitational waves background (SGWB). Moreover, the evidences of the SGWB at nanohz are detected by the pulsar timing arrays (PTA) collaborations, including the North American Nanohertz Observatory for Gravitational Waves (NANOGrav) [15, 16], the European Pulsar Timing Array (EPTA) [17, 18], the Parkes Pulsar Timing Array (PPTA) [19, 20], the International Pulsar Timing Array (IPTA) [21], and the Chinese Pulsar Timing Array (CPTA) [22]. The generation mechanism of SGWB is a highly debated topic with enormous models including supermassive black hole binaries (SMBHBs) [23–26], curvature perturbations [27, 28], and new-physics models such as first-order phase transition (FOPT) [29–47], cosmic strings [48–54], and domain walls [55–64], etc. Amongst the studies, it has been estimated that the SGWB can be induced by a strong FOPT at about $T_* \sim 1 - 10$ MeV [65–67], which makes the cosmic QCD phase transition (PT) a competitive candidate. Moreover, the recent studies suggest that the large lepton asymmetries can induce the QCD FOPT in early Universe, and give the observed value of baryon asymmetry via the so called “sphaleron freeze-in” mechanism [68, 69]. Thus, a strong QCD phase transition may be a simple solution for multiple problems in cosmology.

The nonperturbative nature of QCD makes it difficult to study its PT dynamics, especially when it comes to the quantitative information of thermodynamics quantities and the effective potential of QCD. Recently, the quantitative truncation scheme together with the computation of thermodynamics quantities are reached [70], and a novel method to determine the effective potential was proposed in Ref. [71]. These progresses make the quantitative analysis of the QCD PT viable through the Dyson-Schwinger equation (DSE) [70–75]. For the first time, we quantitatively determine the strength, the duration, and the percolation temperature T_* of the QCD PT. We then compute the gravitational waves (GWs) spectrum from QCD PT and found that the signal from QCD PT is unlikely to match with the NANOGrav measurements and the being constructed GW detectors in the frequency range from nanohertz to hertz.

Cosmic trajectories In the QCD epoch, the baryon number Y_B , the individual lepton flavour number Y_{L_f} , and the electric charge Q asymmetry can be considered as the conserved quantities during the QCD PT [76]. Thus, without any further assumptions, one can consider the conservation equations:

$$Y_{L_f} = \frac{n_f + n_{\nu_f}}{s}, \quad Y_B = \sum_i \frac{B_i n_i}{s}, \quad Q = \sum_i \frac{Q_i n_i}{s}, \quad (1)$$

with s the total entropy density of the Universe, n_i the net number density (i.e., the particle minus the anti-particle number density of the species i), $f = (e, \mu, \tau)$, $i = (e, \mu, \tau, u, d, s, c)$, B_i the baryon number of species i , Q_i the electric charge of species i , $Y_B = 8.7 \times 10^{-11}$ the observed baryon asymmetry [77], $Q = 0$ the charge neutrality for universe. Y_{L_f} is less constrained, allowing for a larger lepton asymmetry, provided it satisfies the big bang nucleosynthesis (BBN) and the cosmic microwave background (CMB) constraint $|Y_{L_e} + Y_{L_\mu} + Y_{L_\tau}| < 1.2 \times$

* zhenghuiwen@stu.pku.edu.cn

† fei.gao@bit.edu.cn

‡ lgbycl@cqu.edu.cn

§ sqin@cqu.edu.cn

¶ yxliu@pku.edu.cn

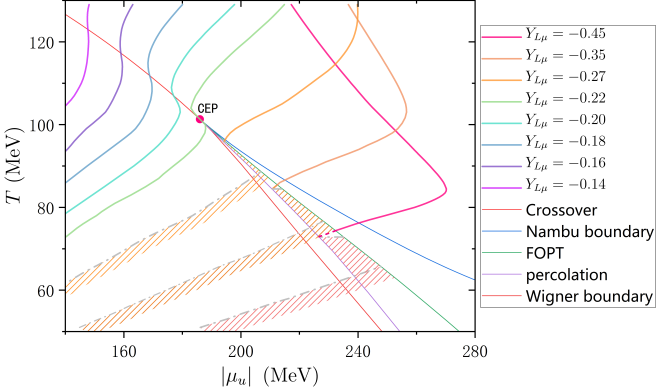


FIG. 1. Cosmic trajectories in the scenario $Y_{L_e} = 0$ and $Y_{L_\mu} = -Y_{L_\tau}$ in QCD phase diagram. The cosmic trajectories intersect the FOPT line at (T_c, μ_c) and the percolation line at (T_*, μ_*) . Solid line: the determined cosmic trajectory; dashed line: the supercooling stage for a cosmic trajectory before the percolation and after the FOPT; gray dot-dashed line: the upper bound for the possible cosmic trajectory; shadow region: an area contains possible cosmic trajectory.

10^{-2} [78–83]. Under this constraint, the individual Y_{L_f} will decrease once the neutrino oscillations start at $T_* \sim 10$ MeV [84–86]. Therefore, the large lepton asymmetries exist only for $T_* > 10$ MeV. For $T_* < 10$ MeV, the diminished Y_{L_f} will lower the lepton and the quark chemical potentials to satisfy the BBN constraint.

Under the conditions of the kinetic and the chemical equilibrium [76], the net leptons and the photons number densities are expressed by Fermi-Dirac distributions and Bose-Einstein distributions, respectively. In the QCD sector, the nonperturbative property prevents the QCD matter from being simply represented by the free particle distributions. Therefore, we apply the DSE to accomplish the complete calculations of the QCD phase diagram, the thermodynamic quantities and especially here the effective potential, which is for the first time obtained and applied to compute the gravitational wave signals.

This work focuses on the scenario $(Y_{L_e} = 0, Y_{L_\mu} = -Y_{L_\tau})$, which satisfies BBN constraints and can induce the QCD FOPT [68, 87]. Fig. 1 shows how the cosmic trajectory depends on Y_{L_μ} . The critical value $Y_{L_\mu} = -0.22$ triggers the FOPT, which is consistent with the previous study [69]. As Y_{L_μ} decreases from -0.14 to -0.22 , the cosmic trajectory quickly approaches the CEP. When $Y_{L_\mu} < -0.22$, the trajectory enters the FOPT region.

When the cosmic trajectory crosses the FOPT, there can be GW emission during the bubble nucleation. Before nucleation, the QCD effective potential, explained in the next section, can be used to study the process. After nucleation, when part of the Universe is converted to the true vacuum, the entropy is no longer conserved due to the non-equilibrium effect. The upper bound of the cosmic trajectory is determined under the condition that s/n_q is conserved after the PT as shown in Fig. 1. The evolution after the percolation stage is influenced by

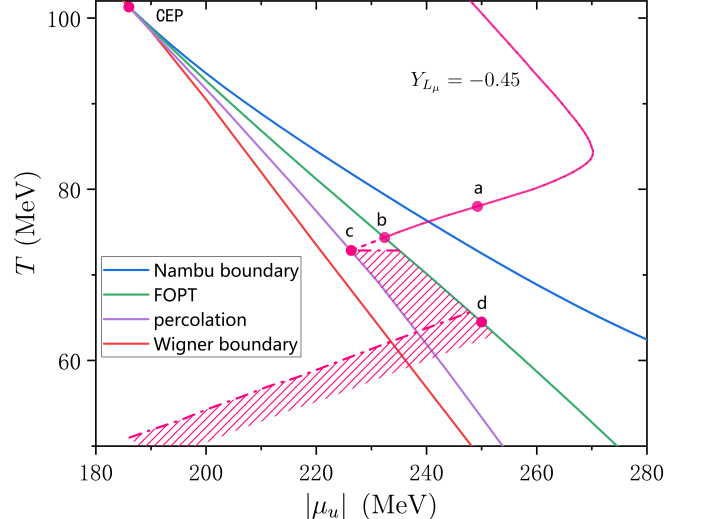


FIG. 2. The cosmic trajectory across the FOPT region in the scenario $Y_{L_e} = 0, Y_{L_\mu} = -Y_{L_\tau}$, where $Y_{L_\mu} = -0.45$. Solid line: the determined cosmic trajectory, such as $a-b$; dashed line: the supercooling stage for a cosmic trajectory before the percolation and after the FOPT, such as $b-c$; dot-dashed line: the upper bound for the possible cosmic trajectory; shadow region: an area contains possible cosmic trajectory.

the dynamics of the bubble expansion, the increase in total entropy in the system due to non-equilibrium processes, and their interplay. The bubble expansion modifies the volume fraction of the true vacuum within the Hubble volume after percolation, which in turn affects extensive thermodynamic quantities. Meanwhile, the increase in total entropy, driven by non-equilibrium processes, causes the evolution to deviate from equilibrium. Both have significant impacts on conservation laws, making the determination of the cosmic trajectory challenging, with only the upper limit of the stage after percolation being determined. Nevertheless, our main focus is the GW signals generated during the percolation stage, which can be fully determined within the information before the percolation stage.

We illustrate the detailed evolution in Fig. 2 with $Y_{L_\mu} = -0.45$ along the path. During the $a-b$ period, the symmetric vacuum energy is lower. At this stage, the universe is filled with the symmetric vacuum, i.e., the Wigner vacuum in QCD. In the subsequent $b-c$ period, the energy of the Wigner vacuum exceeds that of Nambu vacuum, yet both are in local minima. This is then a supercooling period with the universe remaining in Wigner vacuum. At the point c , the Wigner vacuum initiates the decay into the true vacuum, leading to the nucleation and the percolation of bubbles. The $c-d$ process remains unclear due to the absence of calculations for non-equilibrium effects. However, cosmic trajectories involving these processes are constrained within the shaded region. The dot-dashed line above point d marks the upper bound of the cosmic trajectory determined by the true vacuum under the conservation of s/n , while

s/n generally increases due to the non-equilibrium effects. Near point d , the Gibbs phase equilibrium condition requires the cosmic trajectory aligns with the FOPT line. At point d , the Universe is filled with the Nambu vacuum, marking the end of the phase transition.

PT parameters. The QCD FOPT mechanism is expected to generate gravitational waves (GWs). To account for the causality tail in GW signals [88], we apply the GW spectrum modeled by NANOGrav. The GW spectrum is written as [65, 89–95]:

$$\Omega_b(f) = \mathcal{D} \tilde{\Omega}_b \left(\frac{\kappa_b \alpha_*}{1 + \alpha_*} \right)^2 (H_* R_*)^2 S(f/f_b), \quad (2)$$

$$\Omega_s(f) = \mathcal{D} \tilde{\Omega}_s \Upsilon(\tau_{sw}) \left(\frac{\kappa_s \alpha_*}{1 + \alpha_*} \right)^2 (H_* R_*) \mathcal{S}(f/f_s), \quad (3)$$

with α_* the PT strength, $\beta/H_* = (8\pi)^{1/3} v_w/(H_* R_*)$ being the inverse PT duration [91] and v_w the bubble wall velocity. Both parameters requires the knowledge of the QCD effective potential, which we obtain by applying the homotopy method to the QCD theory [71]. The PT parameters are calculated on the percolation line, which corresponds to the percolation temperature T_* , i.e., the temperature when $\sim 34\%$ of the volume of the universe is converted into the true vacuum determined with the effective potential.

The QCD effective potential comes from a generalized Legendre transformation to the Cornwall, Jackiw and Tomboulis (CJT) generating functional [71]. This transformation converts the variable of the CJT effective potential, i.e., the quark propagator, to the self-energy, which is the key point to keep the effective potential to be bounded from below [96]. The new effective potential is written as [71]:

$$\Gamma_\Sigma[\Sigma] = \text{Tr} \ln [S_0^{-1} + \Sigma]^{-1} - \text{Tr}[1] - \Gamma_2[(S + L)] + \text{Tr}[(S + L)\Sigma], \quad (4)$$

with S_0 the free quark propagator, S the dressed quark propagator, $\Sigma = \Sigma[(S + L)] \equiv \frac{\delta \Gamma_2[(S + L)]}{\delta(S + L)}$ the self-energy, L the external source, and Γ_2 the sum of all two-particle-irreducible diagrams as a functional of $S + L$.

Moreover, we apply the homotopy method, i.e., a simplified version of the functional integration, to determine the effective potential from the quantitative truncation scheme of the DSE [71]:

$$\Gamma_\Sigma[M_q] := \int_0^\chi d\xi \text{Tr} \left\{ \frac{d\Sigma_\xi}{d\xi} \left[-(S_0^{-1} + \Sigma_\xi)^{-1} + S_\xi \right] \right\}, \quad (5)$$

where M_q the dynamic quark mass that depends on the homotopy parameter and

$$\Sigma_\xi = \Sigma[S_\xi], \quad S_\xi = [(1 - \xi)S_1^{-1} + \xi S_2^{-1}]^{-1}, \quad (6)$$

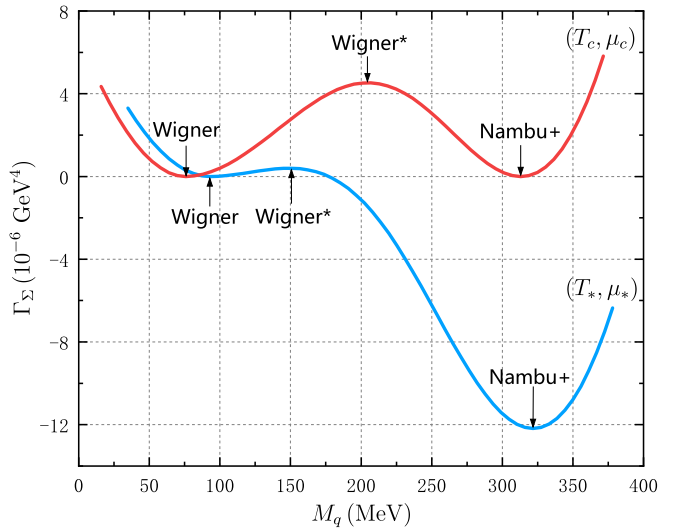


FIG. 3. The $N_f = 2$ effective potential evolving from (T_c, μ_c) to (T_*, μ_*) for the $Y_{L_\mu} = -0.45$ cosmic trajectory. The dynamic quark mass M_q is the order parameter of the effective potential and the effective potential is defined to be zero at the Wigner solution.

with χ and ξ being the homotopy parameter, S_1 and S_2 being the Wigner and Nambu+ solutions, and Σ the self-energy whose explicit expression is placed in the supplement. In the functional space, a one-dimensional line parameterized by χ and ξ , on which the effective potential lies, is chosen.

We illustrate the effective potential Γ_Σ in Fig. 3, where the Wigner vacuum is the false vacuum, the Nambu+ is the true vacuum and the Wigner* is the unstable vacuum indicating the occurrence of FOPT. At the PT temperature T_c , the two vacuums are degenerate. Vacuum bubbles merge around the percolation temperature T_* . At that time, the false vacuum has an energy larger than the other. Since the homotopy method guarantees the functional relation between the effective potential and the equation of motion of QCD, the effective potential incorporates all the information from the non-perturbative DSE, which naturally includes the temperature effects and all the temperature-induced infrared effects.

Using the effective potential, we calculate the decay rate of the false vacuum using the python package [97]:

$$\Gamma(T, \mu) = \frac{\sqrt{|\lambda_-|}}{2\pi} \left| \frac{\det'(-\nabla^2 + V''_{\text{eff}}(\phi_b))}{\det(-\nabla^2 + V''_{\text{eff}}(\phi_F))} \right|^{-1/2} \times \left(\frac{S_3}{2\pi T} \right)^{\frac{3}{2}} \exp \left(-\frac{S_3}{T} \right), \quad (7)$$

with

$$S_3 = 4\pi \int_0^\infty dr r^2 \left[\frac{1}{2} \left(\frac{d\phi_b}{dr} \right)^2 + V_{\text{eff}}(\phi_b) \right]. \quad (8)$$

Here, ϕ_b is the bounce solution, ϕ_F is false vacuum solution, λ_- is the negative eigenvalue of the functional deter-

minant, S_3 is the 3-dimensional Euclidean actions for the $O(3)$ -symmetric bounce solutions, r is the bubble radius, $\phi = M_q$ is the dynamical quark mass, $V''_{\text{eff}} = d^2 V_{\text{eff}} / d\phi^2$, and $V_{\text{eff}} = \Gamma_\Sigma$ is the effective potential calculated from the DSE with the homotopy method [71]. It is important to note that QCD lacks a tree-level potential that describes the dynamical quark mass M_q . Therefore, we must construct an effective theory with M_q as the degrees of freedom and V_{eff} as the tree-level potential. Furthermore, based on this effective theory, we can also incorporate one-loop corrections to V_{eff} . The evolution of the decay rate and the percolation temperature with the evolution details in the supplemental material.

We calculate the bubble wall velocity and find it to be lower than both the Jouguet velocity and the speed of sound in the background radiation, which indicates the subsonic deflagration mode, with details putting in the Supplemental Material. The GW spectrum parameter κ_s is determined as in Ref. [91]. Additionally, the local thermal equilibrium (LTE) effects could influence the bubble wall velocity [98, 99]. They are not included here because α_* is small in our study, which makes the bubble wall velocity highly sensitive to the enthalpy ratio between the broken and symmetric phases (Ψ_n), and introduces significant uncertainty in determining v_w . Since v_w does not qualitatively affect our conclusions on the GW spectrum, LTE corrections are omitted.

The PT strength α_* depends on the available energy released from the PT, normalized to the energy densities of the background radiation:

$$\alpha_* = \frac{\Delta\theta}{\rho_r} \Big|_{(T_*, \mu_*)}, \quad (9)$$

with

$$\Delta\theta = \frac{1}{4} T \Delta s + \frac{1}{4} \mu_q \Delta n_q - \frac{1 + 1/c_{s,b}^2}{4} \Delta P, \quad c_{s,b}^2 = \frac{dp}{de} \Big|_{s,b},$$

$$\rho_r(T, \mu) = \sum_a \int \frac{d^3 p}{(2\pi)^3} E_a f_{F/B}(E_a, T, \mu). \quad (10)$$

Here, $E_a = \sqrt{p^2 + m_a^2}$, θ is the pseudotrace anomaly [100], s is the entropy density, n_q is the quark number density and ρ_r collects electron, muon, all neutrinos, photon and u/d quarks. The $c_{s,b}^2$ is the speed of sound for the Nambu phase, where the derivative is along the Isentropic trajectory, p_b is the respective pressure and e_b is the energy density. A critical value α_∞ that can determine whether the bubble walls can runaway is also considered [93, 101], which also determines the parameter κ_p .

For the FOPT with finite chemical potential, the inverse PT duration β/H_* can be obtained as:

$$\beta/H_* = 4\rho_r \frac{d}{d\rho_r} \left(\frac{S_3}{T} \right) \Big|_{(T_*, \mu_*)}, \quad (11)$$

where the derivative lies along the cosmic trajectory. The details of above equations can be found in the supplementary material. In summary, the QCD effective potential

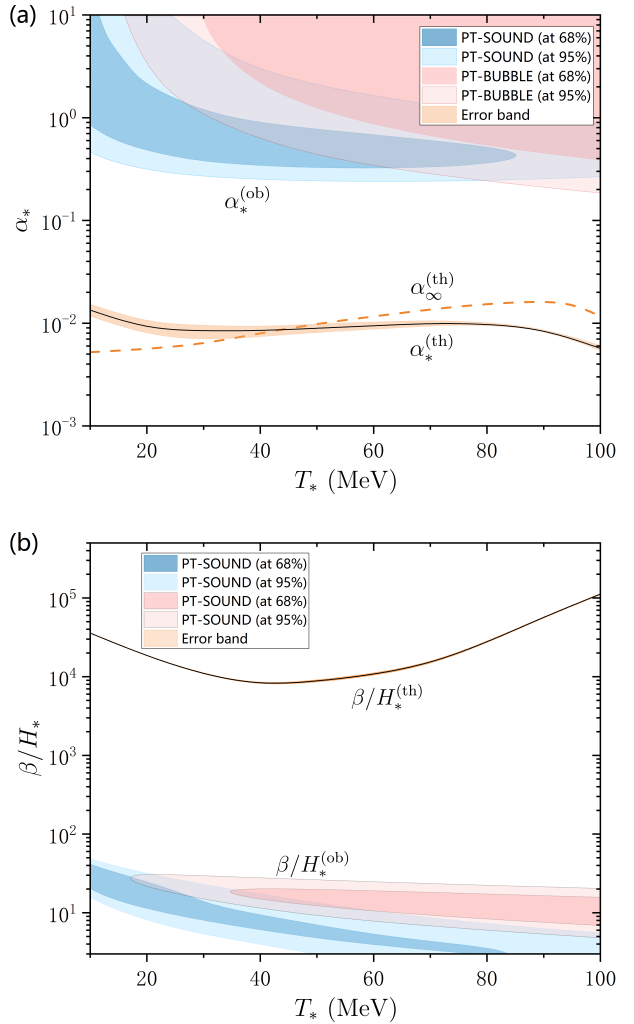


FIG. 4. (a) The PT strength α_* . (b) The inverse PT duration β/H_* . The temperature dependence of α_* and β/H_* is on the percolation line. The shaded region: the NANOGrav constraints for the PT-SOUND and the PT-BUBBLE model [65]. The superscripts of α_* and β/H_* are as follows: "th" denotes theory, and "ob" denotes observation.

completely determines the parameters and the pattern of the GW spectrum as depicted in the next section.

Numerical results. After a complete computation for the GW spectrum, we find that neither α_* and β/H_* over the whole chiral PT can be matched with the NANOGrav measurements as shown in Fig. 4. The error bands in Fig. 4 and Fig. 5, coming from the computation of QCD sector with varying the chiral condensate by 10%, are negligible compared to the uncertainties in the gravitational wave models. After a complete computation for the GW spectrum, we find that neither α_* and β/H_* over the whole chiral PT can be matched with the NANOGrav measurements as shown in Fig. 4. The error bands in Fig. 4 and Fig. 5, coming from the computation of QCD sector with varying the chiral condensate by 10%, are negligible compared to the uncertainties in

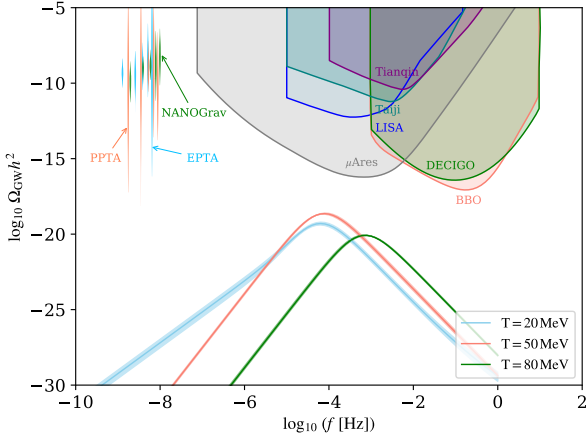


FIG. 5. The GW spectra of the QCD FOPT, where $T = [20, 50, 80]$ MeV correspond to points on the percolation line in the phase diagram. The violins plot the first five frequency bins of the datasets, including: EPTA [18], PPTA [20, 102, 103], and NANOGrav [16, 65, 104]. The sensitivity curves includes: μ Ares [1], Taiji [2, 3], Tianqin [4, 5], LISA [6–9], BBO [10, 11] and DECIGO [12–14].

the gravitational wave models.

In detail, for α_* , its value is at least one order of magnitude smaller compared to the NANOGrav constraints. Such a small value is mainly due to the large energy density of the background radiation. The large energy density comes from the large chemical potentials of the leptons, which is a direct result of the conservation conditions in Eq. (1). In particular, the chemical potentials of the electron and electron neutrino are roughly same as the quark's, while those of muon neutrinos and tau neutrinos are more than three times than the quark's. For β/H_* , the value we obtained is three orders of magnitude larger than the one to match with the analysis from NANOGrav collaboration. This is mainly because the cosmic trajectory leans more towards the chemical potential, causing the derivative of S_3/T along the trajectory to be large. Meanwhile, in the Eq. (11), ρ_r outside of the derivative also maintains a large value due to the contribution of the non-vanishing chemical potential along the percolation line.

Based on the obtained PT parameters α_* and β/H_* , we show our result of the GWs sourced from the QCD FOPT in Fig. 5. To be specific, for $T_* > 42.9$ MeV, where $\alpha < \alpha_\infty$, we only consider the PT-SOUND model from the NANOGrav. for $T_* < 42.9$ MeV, where $\alpha > \alpha_\infty$, both the bubble collision and the sound wave effects are

taken into account for the GW spectrum. The quantitative computation here disapproves the QCD first-order chiral phase transition as a source of the SGWB to explain the signals detected by NANOGrav.

Conclusion. In this *Letter*, we calculate the cosmic trajectories at large quark chemical potential, and for the first time quantitatively determine the PT parameters of the QCD FOPT, through their relation to the thermodynamic quantities and effective potential from the DSE.

We firstly verify that a large lepton asymmetry can induce the QCD FOPT. We consider the scenario ($Y_{L_e} = 0, Y_{L_\mu} = -Y_{L_\tau}$), and find that the FOPT occurs when $Y_{L_\mu} < -0.22$. This conclusion is essentially from the conservation laws during the Universe evolution without further assumptions. We further compute the PT parameters via the QCD effective potential, and then determine the GW spectrum through the sound shell model.

The obtained PT strength α_* is $\mathcal{O}(10^{-2})$, the inverse PT duration β/H_* is $\mathcal{O}(10^4)$. The values deviate significantly from the measurements of NANOGrav mainly due to the large energy density of the background radiation. This large energy density arises from the large chemical potentials of the leptons, which is a direct result of the conservation laws. We compare the GW spectra computed from PT parameters with violin plots and GW detector sensitivity curves. Our analysis shows that the SGWB signal from the QCD chiral FOPT is too weak for detection by NANOGrav or current and upcoming GW detectors.

Additionally, it may be worth exploring the scenario in Ref. [105–109], which provides an exit of electroweak (EW) supercooling with QCD phase transition. This involves a beyond-Standard-Model (BSM) scalar field that acts as the coefficient of the Higgs field's quadratic term. The consequences are twofold: first, EW symmetry remains unbroken until the QCD FOPT occurs, resulting in a QCD phase transition with six massless quarks and a critical endpoint (CEP) at lower chemical potential; Second, the breaking of the Higgs and BSM fields releases significant vacuum energy, potentially exceeding the energy density of the thermal bath, which could produce detectable gravitational waves.

Acknowledgments F.G. and H.Z. thank Isabel M. Oldengott and Yi Lu for helpful discussions. This work is supported by the National Science Foundation of China under Grants No.12175007, No.12247107 and No.12305134. L.B. is supported by the National Natural Science Foundation of China (NSFC) under Grants No. 12075041, No. 12322505, and No. 12347101. L.B. also acknowledges Chongqing Talents: Exceptional Young Talents Project No. cstc2024ycjh-bgzxm0020.

[1] A. Sesana et al., *Exper. Astron.* **51**, 1333 (2021), arXiv:1908.11391 [astro-ph.IM].

[2] W.-R. Hu and Y.-L. Wu, *Natl. Sci. Rev.* **4**, 685 (2017).

- [3] W.-H. Ruan, Z.-K. Guo, R.-G. Cai, and Y.-Z. Zhang, *Int. J. Mod. Phys. A* **35**, 2050075 (2020), arXiv:1807.09495 [gr-qc].
- [4] J. Luo et al. (TianQin), *Class. Quant. Grav.* **33**, 035010 (2016), arXiv:1512.02076 [astro-ph.IM].
- [5] K. Zhou, J. Cheng, and L. Ren, (2023), arXiv:2306.14439 [gr-qc].
- [6] P. Amaro-Seoane et al. (LISA), (2017), arXiv:1702.00786 [astro-ph.IM].
- [7] J. Baker et al., (2019), arXiv:1907.06482 [astro-ph.IM].
- [8] G. Boileau, A. C. Jenkins, M. Sakellariadou, R. Meyer, and N. Christensen, *Phys. Rev. D* **105**, 023510 (2022), arXiv:2109.06552 [gr-qc].
- [9] K. Schmitz, *Symmetry* **12**, 1477 (2020), arXiv:2005.10789 [hep-ph].
- [10] J. Crowder and N. J. Cornish, *Phys. Rev. D* **72**, 083005 (2005), arXiv:gr-qc/0506015.
- [11] G. M. Harry, P. Fritschel, D. A. Shaddock, W. Folkner, and E. S. Phinney, *Class. Quant. Grav.* **23**, 4887 (2006), [Erratum: Class.Quant.Grav. 23, 7361 (2006)].
- [12] N. Seto, S. Kawamura, and T. Nakamura, *Phys. Rev. Lett.* **87**, 221103 (2001), arXiv:astro-ph/0108011.
- [13] K. Yagi and N. Seto, *Phys. Rev. D* **83**, 044011 (2011), [Erratum: Phys.Rev.D 95, 109901 (2017)], arXiv:1101.3940 [astro-ph.CO].
- [14] S. Isoyama, H. Nakano, and T. Nakamura, *PTEP* **2018**, 073E01 (2018), arXiv:1802.06977 [gr-qc].
- [15] Z. Arzoumanian et al. (NANOGrav), *Astrophys. J. Lett.* **905**, L34 (2020), arXiv:2009.04496 [astro-ph.HE].
- [16] G. Agazie et al. (NANOGrav), *Astrophys. J. Lett.* **951**, L8 (2023), arXiv:2306.16213 [astro-ph.HE].
- [17] S. Chen et al. (EPTA), *Mon. Not. Roy. Astron. Soc.* **508**, 4970 (2021), arXiv:2110.13184 [astro-ph.HE].
- [18] J. Antoniadis et al. (EPTA, InPTA:), *Astron. Astrophys.* **678**, A50 (2023), arXiv:2306.16214 [astro-ph.HE].
- [19] B. Goncharov et al., *Astrophys. J. Lett.* **917**, L19 (2021), arXiv:2107.12112 [astro-ph.HE].
- [20] D. J. Reardon et al., *Astrophys. J. Lett.* **951**, L6 (2023), arXiv:2306.16215 [astro-ph.HE].
- [21] J. Antoniadis et al., *Mon. Not. Roy. Astron. Soc.* **510**, 4873 (2022), arXiv:2201.03980 [astro-ph.HE].
- [22] H. Xu et al., *Res. Astron. Astrophys.* **23**, 075024 (2023), arXiv:2306.16216 [astro-ph.HE].
- [23] M. Rajagopal and R. W. Romani, *Astrophys. J.* **446**, 543 (1995), arXiv:astro-ph/9412038.
- [24] E. S. Phinney, (2001), arXiv:astro-ph/0108028.
- [25] A. H. Jaffe and D. C. Backer, *Astrophys. J.* **583**, 616 (2003), arXiv:astro-ph/0210148.
- [26] J. S. B. Wyithe and A. Loeb, *Astrophys. J.* **590**, 691 (2003), arXiv:astro-ph/0211556.
- [27] K. N. Ananda, C. Clarkson, and D. Wands, *Phys. Rev. D* **75**, 123518 (2007), arXiv:gr-qc/0612013.
- [28] D. Baumann, P. J. Steinhardt, K. Takahashi, and K. Ichiki, *Phys. Rev. D* **76**, 084019 (2007), arXiv:hep-th/0703290.
- [29] M. Losada, *Phys. Rev. D* **56**, 2893 (1997), arXiv:hep-ph/9605266.
- [30] J. M. Cline and P.-A. Lemieux, *Phys. Rev. D* **55**, 3873 (1997), arXiv:hep-ph/9609240.
- [31] A. Neronov, A. Roper Pol, C. Caprini, and D. Semikoz, *Phys. Rev. D* **103**, 041302 (2021), arXiv:2009.14174 [astro-ph.CO].
- [32] S. L. Li, L. J. Shao, P. X. Wu, and H. Yu, *Phys. Rev. D* **104**, 043510 (2021), arXiv:2101.08012 [astro-ph.CO].
- [33] Y. Nakai, M. Suzuki, F. Takahashi, and M. Yamada, *Phys. Lett. B* **816**, 136238 (2021), arXiv:2009.09754 [astro-ph.CO].
- [34] W. Ratzinger and P. Schwaller, *SciPost Phys.* **10**, 047 (2021), arXiv:2009.11875 [astro-ph.CO].
- [35] A. Kosowsky, M. S. Turner, and R. Watkins, *Phys. Rev. Lett.* **69**, 2026 (1992).
- [36] C. Caprini, R. Durrer, and X. Siemens, *Phys. Rev. D* **82**, 063511 (2010), arXiv:1007.1218 [astro-ph.CO].
- [37] X. Xue et al., *Phys. Rev. Lett.* **127**, 251303 (2021), arXiv:2110.03096 [astro-ph.CO].
- [38] J. Ellis, M. Lewicki, C. Lin, and V. Vaskonen, *Phys. Rev. D* **108**, 103511 (2023), arXiv:2306.17147 [astro-ph.CO].
- [39] A. Addazi, Y.-F. Cai, A. Marciano, and L. Visinelli, *Phys. Rev. D* **109**, 015028 (2024), arXiv:2306.17205 [astro-ph.CO].
- [40] T. Ghosh, A. Ghoshal, H.-K. Guo, F. Hajkarim, S. F. King, K. Sinha, X. Wang, and G. White, *JCAP* **05**, 100 (2024), arXiv:2307.02259 [astro-ph.HE].
- [41] S. Rezapour, K. Bitaghirs Fadafan, and M. Ahmadvand, *Phys. Scripta* **97**, 035301 (2022).
- [42] M. Ahmadvand and K. Bitaghirs Fadafan, *Phys. Lett. B* **772**, 747 (2017), arXiv:1703.02801 [hep-th].
- [43] P. Athron, A. Fowlie, C.-T. Lu, L. Morris, L. Wu, Y. Wu, and Z. Xu, *Phys. Rev. Lett.* **132**, 221001 (2024), arXiv:2306.17239 [hep-ph].
- [44] C. Han, K.-P. Xie, J. M. Yang, and M. Zhang, (2023), arXiv:2306.16966 [hep-ph].
- [45] A. Salvio, *Phys. Lett. B* **852**, 138639 (2024), arXiv:2312.04628 [hep-ph].
- [46] R. Qin and L. Bian, (2024), arXiv:2407.01981 [hep-ph].
- [47] Y. Gouttenoire, *Phys. Rev. Lett.* **131**, 171404 (2023), arXiv:2307.04239 [hep-ph].
- [48] X. Siemens, V. Mandic, and J. Creighton, *Phys. Rev. Lett.* **98**, 111101 (2007), arXiv:astro-ph/0610920.
- [49] S. Blasi, V. Brdar, and K. Schmitz, *Phys. Rev. Lett.* **126**, 041305 (2021), arXiv:2009.06607 [astro-ph.CO].
- [50] W. Buchmuller, V. Domcke, and K. Schmitz, *Phys. Lett. B* **811**, 135914 (2020), arXiv:2009.10649 [astro-ph.CO].
- [51] G. Lazarides, R. Maji, and Q. Shafi, *Phys. Rev. D* **108**, 095041 (2023), arXiv:2306.17788 [hep-ph].
- [52] Z. Wang, L. Lei, H. Jiao, L. Feng, and Y.-Z. Fan, *Sci. China Phys. Mech. Astron.* **66**, 120403 (2023), arXiv:2306.17150 [astro-ph.HE].
- [53] R. Samanta and S. Datta, *JHEP* **05**, 211 (2021), arXiv:2009.13452 [hep-ph].
- [54] L. Bian, J. Shu, B. Wang, Q. Yuan, and J. Zong, *Phys. Rev. D* **106**, L101301 (2022), arXiv:2205.07293 [hep-ph].
- [55] T. Hiramatsu, M. Kawasaki, and K. Saikawa, *JCAP* **02**, 031 (2014), arXiv:1309.5001 [astro-ph.CO].
- [56] R. Z. Ferreira, A. Notari, O. Pujolas, and F. Rompineve, *JCAP* **02**, 001 (2023), arXiv:2204.04228 [astro-ph.CO].
- [57] N. Kitajima, J. Lee, K. Murai, F. Takahashi, and W. Yin, *Phys. Lett. B* **851**, 138586 (2024), arXiv:2306.17146 [hep-ph].
- [58] S. Blasi, A. Mariotti, A. Rase, and A. Sevrin, *JHEP* **11**, 169 (2023), arXiv:2306.17830 [hep-ph].
- [59] Y. Li, L. Bian, and Y. Jia, (2023), arXiv:2304.05220 [hep-ph].
- [60] L. Bian, S. Ge, C. Li, J. Shu, and J. Zong, (2022), arXiv:2212.07871 [hep-ph].

- [61] E. Babichev, D. Gorbunov, S. Ramazanov, R. Samanta, and A. Vikman, *Phys. Rev. D* **108**, 123529 (2023), arXiv:2307.04582 [hep-ph].
- [62] A. S. Sakharov, Y. N. Eroshenko, and S. G. Rubin, *Phys. Rev. D* **104**, 043005 (2021), arXiv:2104.08750 [hep-ph].
- [63] Z. Zhang, C. Cai, Y.-H. Su, S. Wang, Z.-H. Yu, and H.-H. Zhang, *Phys. Rev. D* **108**, 095037 (2023), arXiv:2307.11495 [hep-ph].
- [64] Y. Gouttenoire and E. Vitagliano, *Phys. Rev. D* **110**, L061306 (2024), arXiv:2306.17841 [gr-qc].
- [65] A. Afzal et al. (NANOGrav), *Astrophys. J. Lett.* **951**, L11 (2023), arXiv:2306.16219 [astro-ph.HE].
- [66] L. Bian, S. Ge, J. Shu, B. Wang, X.-Y. Yang, and J. Zong, *Phys. Rev. D* **109**, L101301 (2024), arXiv:2307.02376 [astro-ph.HE].
- [67] Y. Bai and M. Korwar, *Phys. Rev. D* **105**, 095015 (2022), arXiv:2109.14765 [hep-ph].
- [68] F. Gao and I. M. Oldengott, *Phys. Rev. Lett.* **128**, 131301 (2022), arXiv:2106.11991 [hep-ph].
- [69] F. Gao, J. Harz, C. Hati, Y. Lu, I. M. Oldengott, and G. White, (2023), arXiv:2309.00672 [hep-ph].
- [70] Y. Lu, F. Gao, Y.-X. Liu, and J. M. Pawlowski, *Phys. Rev. D* **110**, 014036 (2024), arXiv:2310.18383 [hep-ph].
- [71] H. W. Zheng, Y. Lu, F. Gao, S. X. Qin, and Y. X. Liu, *Phys. Rev. D* **109**, 114013 (2024), arXiv:2312.00382 [hep-ph].
- [72] C. D. Roberts and A. G. Williams, *Prog. Part. Nucl. Phys.* **33**, 477 (1994), arXiv:hep-ph/9403224.
- [73] R. Alkofer and L. von Smekal, *Phys. Rept.* **353**, 281 (2001), arXiv:hep-ph/0007355.
- [74] C. S. Fischer, *J. Phys. G* **32**, R253 (2006), arXiv:hep-ph/0605173.
- [75] F. Gao, J. Papavassiliou, and J. M. Pawlowski, *Phys. Rev. D* **103**, 094013 (2021), arXiv:2102.13053 [hep-ph].
- [76] D. J. Schwarz and M. Stuke, *JCAP* **11**, 025 (2009), [Erratum: *JCAP* 10, E01 (2010)], arXiv:0906.3434 [hep-ph].
- [77] N. Aghanim et al. (Planck), *Astron. Astrophys.* **641**, A6 (2020), [Erratum: *Astron. Astrophys.* 652, C4 (2021)], arXiv:1807.06209 [astro-ph.CO].
- [78] C. Pitrou, A. Coc, J. P. Uzan, and E. Vangioni, *Phys. Rept.* **754**, 1 (2018), arXiv:1801.08023 [astro-ph.CO].
- [79] I. M. Oldengott and D. J. Schwarz, *EPL* **119**, 29001 (2017), arXiv:1706.01705 [astro-ph.CO].
- [80] L. A. Popa and A. Vasile, *JCAP* **06**, 028 (2008), arXiv:0804.2971 [astro-ph].
- [81] V. Simha and G. Steigman, *JCAP* **08**, 011 (2008), arXiv:0806.0179 [hep-ph].
- [82] P. D. Serpico and G. G. Raffelt, *Phys. Rev. D* **71**, 127301 (2005), arXiv:astro-ph/0506162.
- [83] G. B. Gelmini, M. Kawasaki, A. Kusenko, K. Murai, and V. Takhistov, *JCAP* **09**, 051 (2020), arXiv:2005.06721 [hep-ph].
- [84] S. Pastor, T. Pinto, and G. G. Raffelt, *Phys. Rev. Lett.* **102**, 241302 (2009), arXiv:0808.3137 [astro-ph].
- [85] G. Mangano, G. Miele, S. Pastor, O. Pisanti, and S. Sarikas, *JCAP* **03**, 035 (2011), arXiv:1011.0916 [astro-ph.CO].
- [86] G. Mangano, G. Miele, S. Pastor, O. Pisanti, and S. Sarikas, *Phys. Lett. B* **708**, 1 (2012), arXiv:1110.4335 [hep-ph].
- [87] M. M. Middeldorf-Wygas, I. M. Oldengott, D. Bödeker, and D. J. Schwarz, *Phys. Rev. D* **105**, 123533 (2022), arXiv:2009.00036 [hep-ph].
- [88] G. Franciolini, D. Racco, and F. Rompineve, *Phys. Rev. Lett.* **132**, 081001 (2024), arXiv:2306.17136 [astro-ph.CO].
- [89] R. Jinno and M. Takimoto, *Phys. Rev. D* **95**, 024009 (2017), arXiv:1605.01403 [astro-ph.CO].
- [90] M. Hindmarsh, S. J. Huber, K. Rummukainen, and D. J. Weir, *Phys. Rev. D* **92**, 123009 (2015), arXiv:1504.03291 [astro-ph.CO].
- [91] J. R. Espinosa, T. Konstandin, J. M. No, and G. Servant, *JCAP* **06**, 028 (2010), arXiv:1004.4187 [hep-ph].
- [92] J. Ellis, M. Lewicki, and J. M. No, *JCAP* **07**, 050 (2020), arXiv:2003.07360 [hep-ph].
- [93] J. Ellis, M. Lewicki, J. M. No, and V. Vaskonen, *JCAP* **06**, 024 (2019), arXiv:1903.09642 [hep-ph].
- [94] H. K. Guo, K. Sinha, D. Vagie, and G. White, *JCAP* **01**, 001 (2021), arXiv:2007.08537 [hep-ph].
- [95] D. J. Weir, *Phil. Trans. Roy. Soc. Lond. A* **376**, 20170126 (2018), [Erratum: *Phil. Trans. Roy. Soc. Lond. A* 381, 20230212 (2023)], arXiv:1705.01783 [hep-ph].
- [96] R. W. Haymaker, T. Matsuki, and F. Cooper, *Phys. Rev. D* **35**, 2567 (1987).
- [97] A. Ekstedt, O. Gould, and J. Hirvonen, *JHEP* **12**, 056 (2023), arXiv:2308.15652 [hep-ph].
- [98] W.-Y. Ai, B. Laurent, and J. van de Vis, *JCAP* **07**, 002 (2023), arXiv:2303.10171 [astro-ph.CO].
- [99] T. Krajewski, M. Lewicki, and M. Zych, *JHEP* **05**, 011 (2024), arXiv:2402.15408 [astro-ph.CO].
- [100] F. Giese, T. Konstandin, and J. van de Vis, *JCAP* **07**, 057 (2020), arXiv:2004.06995 [astro-ph.CO].
- [101] D. Bodeker and G. D. Moore, *JCAP* **05**, 009 (2009), arXiv:0903.4099 [hep-ph].
- [102] D. J. Reardon et al., *Astrophys. J. Lett.* **951**, L7 (2023), arXiv:2306.16229 [astro-ph.HE].
- [103] A. Zic et al., *Publ. Astron. Soc. Austral.* **40**, e049 (2023), arXiv:2306.16230 [astro-ph.HE].
- [104] G. Agazie et al. (NANOGrav), *Astrophys. J. Lett.* **951**, L9 (2023), arXiv:2306.16217 [astro-ph.HE].
- [105] D. Bödeker, *Phys. Rev. D* **104**, L111501 (2021), arXiv:2108.11966 [hep-ph].
- [106] L. Sagunski, P. Schicho, and D. Schmitt, *Phys. Rev. D* **107**, 123512 (2023), arXiv:2303.02450 [hep-ph].
- [107] F. Giese, T. Konstandin, K. Schmitz, and J. van de Vis, *JCAP* **01**, 072 (2021), arXiv:2010.09744 [astro-ph.CO].
- [108] B. von Harling and G. Servant, *JHEP* **01**, 159 (2018), arXiv:1711.11554 [hep-ph].
- [109] S. Iso, P. D. Serpico, and K. Shimada, *Phys. Rev. Lett.* **119**, 141301 (2017), arXiv:1704.04955 [hep-ph].
- [110] F. Gao and J. M. Pawlowski, *Phys. Rev. D* **102**, 034027 (2020), arXiv:2002.07500 [hep-ph].
- [111] O. Philipsen, *Prog. Part. Nucl. Phys.* **70**, 55 (2013), arXiv:1207.5999 [hep-lat].
- [112] J. N. Guenther, R. Bellwied, S. Borsanyi, Z. Fodor, S. D. Katz, A. Pasztor, C. Ratti, and K. K. Szabó, *Nucl. Phys. A* **967**, 720 (2017), arXiv:1607.02493 [hep-lat].
- [113] F. Gao, J. Chen, Y. X. Liu, S. X. Qin, C. D. Roberts, and S. M. Schmidt, *Phys. Rev. D* **93**, 094019 (2016), arXiv:1507.00875 [nucl-th].
- [114] P. Isserstedt, M. Buballa, C. S. Fischer, and P. J. Gunkel, *Phys. Rev. D* **100**, 074011 (2019), arXiv:1906.11644 [hep-ph].
- [115] W. J. Fu and J. M. Pawlowski, *Phys. Rev. D* **92**, 116006 (2015), arXiv:1508.06504 [hep-ph].

- [116] Y. Lu, F. Gao, B. C. Fu, H. C. Song, and Y. X. Liu, (2023), arXiv:2310.16345 [hep-ph].
- [117] C. S. Fischer, J. Luecker, and C. A. Welzbacher, Phys. Rev. D **90**, 034022 (2014), arXiv:1405.4762 [hep-ph].
- [118] A. Eichhorn, J. Lumma, J. M. Pawłowski, M. Reichert, and M. Yamada, JCAP **05**, 006 (2021), arXiv:2010.00017 [hep-ph].
- [119] M. Lewicki, M. Merchand, and M. Zych, JHEP **02**, 017 (2022), arXiv:2111.02393 [astro-ph.CO].
- [120] M. Kamionkowski, A. Kosowsky, and M. S. Turner, Phys. Rev. D **49**, 2837 (1994), arXiv:astro-ph/9310044.
- [121] P. J. Steinhardt, Phys. Rev. D **25**, 2074 (1982).
- [122] J. Ellis, M. Lewicki, and J. M. No, JCAP **04**, 003 (2019), arXiv:1809.08242 [hep-ph].

Supplemental Material

I. THERMAL QUANTITIES AND COSMIC TRAJECTORY DURING THE QCD TRANSITION

At finite temperature and chemical potential, the general form of the solution of the quark DSE can be expressed as:

$$S^{-1}(\tilde{\omega}_n, \vec{p}) = i\vec{\gamma} \cdot \vec{p} A(\tilde{\omega}_n, \vec{p}) + i\gamma_4 \tilde{\omega}_n C(\tilde{\omega}_n, \vec{p}) + B(\tilde{\omega}_n, \vec{p}). \quad (12)$$

with \vec{p} the momentum, $\tilde{\omega}_n = \omega_n + i\mu_q$, $\omega_n = (2n+1)\pi T$ the Matsubara frequency and μ_q the quark chemical potential. Then, the dynamic quark mass is defined as:

$$M_q = \text{Re} \left[\frac{B(\tilde{\omega}_0, \vec{p} = 0)}{C(\tilde{\omega}_0, \vec{p} = 0)} \right]. \quad (13)$$

At finite temperature and chemical potential, the quark gap equation can be written as:

$$S^{-1}(\tilde{\omega}_n, \vec{p}) = (i\gamma_4 \tilde{\omega}_n + i\vec{\gamma} \cdot \vec{p}) + m_\zeta + \Sigma(\tilde{\omega}_n, \vec{p}) \quad (14)$$

with self energy [72]:

$$\Sigma(\tilde{\omega}_n, \vec{p}) = \frac{4}{3} g^2 T \sum_{m=-\infty}^{\infty} \int_q^\Lambda D_{\mu\nu}(\Omega_{nm}, \vec{k}; T, \mu_q) \gamma_\mu S(\tilde{\omega}_m, \vec{q}) \Gamma_\nu(\tilde{\omega}_n, \vec{p}, \tilde{\omega}_m, \vec{q}; T, \mu_q), \quad (15)$$

which is defined in the Euclidean space, with μ_q the quark chemical potential, $\omega_n = (2n+1)\pi T$ the Matsubara frequency and $\tilde{\omega}_n = \omega_n + i\mu_q$ for the quarks. $\Omega_{nm} = \omega_n - \omega_m$ is the Matsubara frequency of the gluon. m_ζ is the current quark mass at the renormalization point ζ , $\int_q^\Lambda d^3 q / (2\pi)^3$ with Λ the energy scale of the loop momentum regularisation. Finally, Γ_ν is the dressed quark-gluon interaction vertex and $D_{\mu\nu}^{ab}$ is the dressed gluon propagator.

The dressed gluon propagator is fitted from the lattice results, and its general form in finite temperature and density is:

$$D_{\mu\nu}(\Omega_{nm}, \vec{k}) = P_{\mu\nu}^T D_T(\Omega_{nm}, \vec{k}) + P_{\mu\nu}^L D_L(\Omega_{nm}, \vec{k}), \quad (16)$$

where $P_{\mu\nu}^{L,T}$ are the longitudinal and transverse projection operators:

$$P_{\mu\nu}^T = (1 - \delta_{\mu 4})(1 - \delta_{\nu 4})(\delta_{\mu\nu} - \frac{k_\mu k_\nu}{k^2}), \quad P_{\mu\nu}^L = (\delta_{\mu\nu} - \frac{k_\mu k_\nu}{k^2}) - P_{\mu\nu}^T, \quad (17)$$

where $k = (\Omega_{nm}, \vec{k})$.

Taking the gauge symmetry in consideration, including the longitudinal and transverse Ward-Green-Takahashi identity, we take the minimal *Ansätze* of the dressed quark-gluon interaction vertex as [110]:

$$\Gamma_\mu(\tilde{\omega}_n, \vec{p}, \tilde{\omega}_m, \vec{q}) = F(k^2) \frac{A(\tilde{\omega}_n, \vec{p}) + A(\tilde{\omega}_m, \vec{q})}{2} \gamma_\mu + Z_{A,L}^{-1/2}(k^2) \Delta_B P_{\mu\nu}^L \sigma_{\mu\nu} k_\nu + Z_{A,T}^{-1/2}(k^2) \Delta_B P_{\mu\nu}^T \sigma_{\mu\nu} k_\nu \quad (18)$$

with

$$\Delta_B = \frac{\tilde{B}(\tilde{\omega}_n, \vec{p}) - \tilde{B}(\tilde{\omega}_m, \vec{q})}{\tilde{\omega}_n^2 + \vec{p}^2 - \tilde{\omega}_m^2 - \vec{q}^2}, \quad \tilde{B}(\tilde{\omega}_n, \vec{p}) = B(\omega_0 \text{ sgn}(\omega_n) + i\mu_q, l_p), \quad (19)$$

where $k = (\Omega_{nm}, \vec{q} - \vec{p})$, $l_p = (\vec{p}^2 + \omega_n^2 - \omega_0^2)^{1/2}$, $Z_{A,L} = D_L(k^2)k^2$ and $Z_{A,T} = D_T(k^2)k^2$ are the gluon dressing functions, and $F(k^2)$ is the ghost dressing function that is fitted from the functional renormalization group (fRG). To include the gluon pressure, we use the lattice QCD results to obtain the entropy density at vanishing chemical potential as parametrized in the lattice QCD [111]. The full entropy density can then be expressed as:

$$s_{QCD}(T, \mu) = s_{latt}(T, \mu = 0) + \delta s(T, \mu). \quad (20)$$

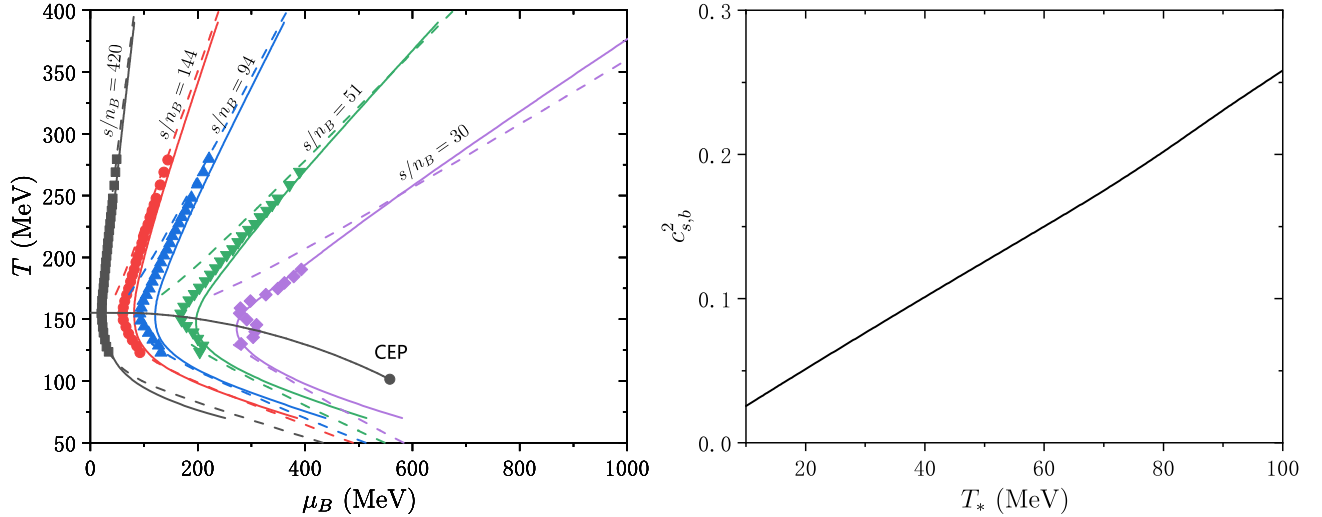


FIG. 6. left panel: Isentropic trajectories at $s/n_B = 420, 144, 94, 51$ and 30 . Solid line: DSE from this work; scatter points: the lattice [112]; dashed line (above): the improved ideal quark gas; dashed line (below): HRG. The solid line with a point represents the crossover of QCD phase transition, with the point corresponding to the critical end point (CEP).right panel: The speed of sound $c_{s,b}^2$ of the broken phase along the percolation line.

The thermal quantities of QCD, including the number density and the entropy density, can be obtained by solving DSE [70, 113, 114]. The quark number density n_q and the entropy s can be written as:

$$n_q = \frac{\partial P}{\partial \mu_q}, \quad s = \frac{\partial P}{\partial T}, \quad (21)$$

with P the pressure and μ_q the quark chemical potential. The number density of u/d and s quark can be expressed in terms of the dynamical quark mass M_q and the traced Polyakov loop Φ in phase diagram (T, μ_q) plane [115, 116]:

$$n_q(T, \mu_q) = 2N_c \int \frac{d^3 k}{(2\pi)^3} [f_q^+(k; T, \mu_q) - f_q^-(k; T, \mu_q)], \quad (22a)$$

$$f_q^\pm(k; T, \mu_q) = \frac{\Phi(T, \mu_q)x_\pm^2 + 2\Phi(T, \mu_q)x_\pm + 1}{x_\pm^3 + 3\Phi(T, \mu_q)x_\pm^2 + 3\Phi(T, \mu_q)x_\pm + 1}, \quad (22b)$$

$$\text{with } x_\pm(k; T, \mu_q) = \exp[(E_q(k; T, \mu_q) \mp \mu_q)/T], \quad E_q(k; T, \mu_q) = \sqrt{k^2 + M_q^2},$$

and with N_c the color number. The traced Polyakov loop Φ at vanishing quark chemical potential is parameterized as [116, 117]:

$$\Phi(T, \mu_q) = L(t_{\mu_q}), \quad (23a)$$

$$t_{\mu_q} = \frac{T}{T_c(0)} + \kappa \left(\frac{3\mu_q}{T_c(0)} \right)^2, \quad L(t) = \frac{2}{1 + \exp \left(\frac{a_1 + b_1 t^3}{t + c_1 t^3 + d_1 t^6} \right)}, \quad (23b)$$

where $T_c(0) = 155.2$ MeV the PT temperature at vanishing chemical potential and $\kappa = 0.0184$ the curvature of the transition line. The fit parameters are $[a_1, b_1, c_1, d_1] = [2.5996, -0.2046, -1.2346, 2.2308]$. From the definition of the Eqs. (21), the chemical potential dependence of the entropy density can be expressed as the integral along μ_q [70]:

$$\delta s(T, \mu) = s(T, \mu) - s(T, 0) = \int_0^{\mu_q} d\mu_q' \frac{\partial n_q(T, \mu')}{\partial T}. \quad (24)$$

Besides, the pseudotrace anomaly takes into account the speed of sound, $c_{s,b}^2$ of the broken phase, which is written as:

$$c_{s,b}^2 = \left. \frac{dp_b}{de_b} \right|_s, \quad (25)$$

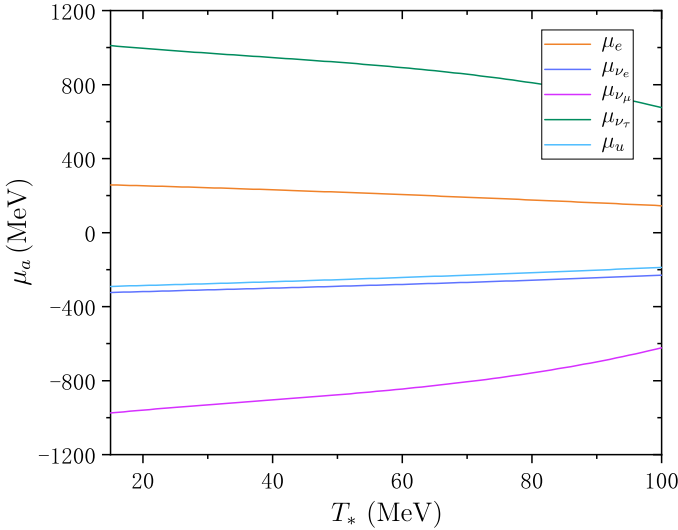


FIG. 7. Chemical potentials of e , μ_e , μ_μ , μ_τ , u when the cosmic trajectories of different Y_{L_μ} reach percolation.

with p_b the pressure density of the broken phase, e_b the energy density of the broken phase and s the fixed entropy density. As shown in Fig. 6, $c_{s,b}^2$ is smaller at lower temperatures, leading to a pseudotrace anomaly that is larger than the traditional trace anomaly.

We compare the isentropic trajectories $s/n_B = \text{const}$ from DSE with the result of the improved ideal quark gas, HRG and the lattice in Fig. (6), showing an well consistency. The improved ideal quark gas includes the lattice QCD entropy $s_{latt}(T, \mu = 0)$ in Eq. (20), and apply the Fermi-Dirac distribution for the quark number densities. The application of $s_{latt}(T, \mu = 0)$ is due to the gluons do not behave like the idea gas in the QCD phase transition region. The consistency shown in Fig. (6) makes the calculation of the five conservation equations of the cosmic trajectories more reliable, because these equations also satisfies a form similar to $s/n_B = \text{const}$.

During the cosmic QCD transition, the kinetic and the chemical equilibrium are excellent approximation [118]. The $2 \leftrightarrow 2$ process is the primary mechanism, responsible for establishing both kinetic and chemical equilibrium among all particles, which constrains the chemical potentials of leptons as $\mu_\mu = \mu_e - \mu_{\nu_e} + \mu_{\nu_\mu}$, and the leptons and quarks as $\mu_d = \mu_e - \mu_{\nu_e} + \mu_u$. Chemical equilibrium constrains the chemical potentials of different particle species to only five independent chemical potentials for the universe. The chemical potentials of photons and gluons are zero because the numbers of photons and gluons are not conserved. The chemical potentials of particles and antiparticles are equal in magnitude, but opposite in sign. For instance, if a particle has a chemical potential of μ_i , its antiparticle has a chemical potential of $-\mu_i$. Due to flavor mixing, we only need to distinguish the chemical potentials of up and down quarks: $\mu_u = \mu_c = \mu_t$, and $\mu_d = \mu_s = \mu_b$ [76]. Therefore we are left with μ_u , μ_e , μ_{ν_e} , μ_{ν_μ} , μ_{ν_τ} as the independent variables for the cosmic trajectory. Then the chemical potentials of conserved charges (Y_{L_f} , Y_B , Q) can be expressed in terms of particle chemical potential as:

$$\mu_{L_f} = \mu_{\nu_f}, \quad (26a)$$

$$\mu_Q = \mu_u - \mu_d, \quad (26b)$$

$$\mu_B = \mu_u + 2\mu_d. \quad (26c)$$

Then the temperature dependence of the five chemical potentials (μ_{L_f} , μ_Q , μ_B) are the cosmic trajectory. We will focus on the (T, μ_q) plane in QCD phase diagram, especially in the first-order phase transition region, where the CEP locates at $(T^E, \mu_q^E) = (101.3, 186.0)$ MeV.

When the cosmic trajectory starts percolation, the conservation conditions with a large lepton asymmetry Y_{L_μ} result in large lepton chemical potential as shown in Fig. 7. The chemical potentials of e and ν_e are of the same order as that of u quark, while the chemical potentials of ν_μ and ν_τ are more than three times that of u quark. Such large lepton chemical potentials are due to the conservation conditions. This, in turn, results in a large total energy density of the Universe, and then significantly influences the GWs spectrum.

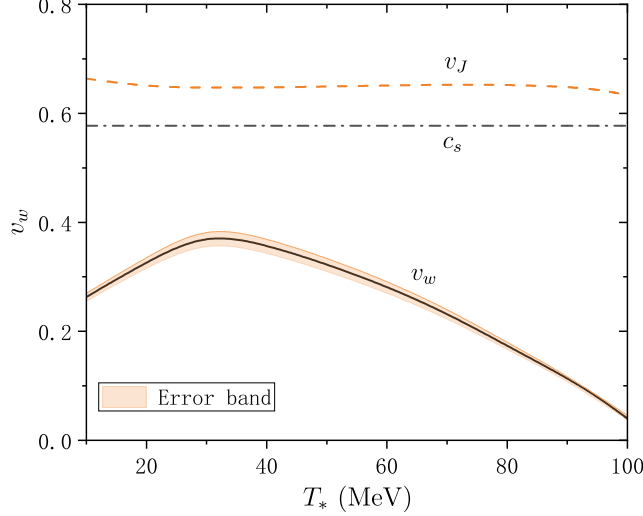


FIG. 8. The bubble wall velocity on the percolation line. Solid line: the bubble wall velocity; dashed line: the Jouquet velocity; dot-dashed line: the speed of sound in the background radiation.

II. PT PARAMETERS OF GRAVITATIONAL WAVES IN FINITE TEMPERATURE AND CHEMICAL POTENTIAL

First one may determine the the bubble wall velocity v_w , as in Ref. [119]:

$$v_w = \begin{cases} \sqrt{\frac{\Delta V_{eff}}{\alpha_* \rho_r}} & \text{for } \sqrt{\frac{\Delta V_{eff}}{\alpha_* \rho_r}} < v_J \\ 1 & \text{for } \sqrt{\frac{\Delta V_{eff}}{\alpha_* \rho_r}} \geq v_J \end{cases}, \quad (27)$$

with v_J the Jouquet velocity as [91, 120, 121]

$$v_J = \frac{1}{\sqrt{3}} \frac{1 + \sqrt{3\alpha_*^2 + 2\alpha_*}}{1 + \alpha_*}. \quad (28)$$

c_s is the speed of sound in the radiation. The results are shown in in Fig. 8.

For the subsonic deflagrations, the efficiency coefficient κ_s that measures how much of the vacuum energy goes into bulk kinetic energy is written as [91]:

$$\kappa_s(v_w \leq c_s) = \frac{c_s^{11/5} \kappa_A \kappa_B}{(c_s^{11/5} - v_w^{11/5}) \kappa_B + v_w c_s^{6/5} \kappa_A}, \quad (29)$$

with

$$\kappa_A = v_w^{6/5} \frac{6.9\alpha_*}{1.36 - 0.037\sqrt{\alpha_*} + \alpha_*}, \quad \kappa_B = \frac{\alpha_*^{2/5}}{0.017 + (0.997 + \alpha_*)^{2/5}}, \quad (30)$$

where α_* is the PT strength, v_w is the bubble wall velocity and c_s is the sound speed in the radiation.

A critical value of α , which can determine whether the bubble walls can runaway, is defined as [93]:

$$\alpha_\infty = \frac{\Delta P_{LO}}{\rho_r}, \quad (31)$$

where [101]

$$\Delta P_{LO} = \sum_{a'} \int_{m_f}^{m_t} dm^2 \int \frac{d^3 p}{(2\pi)^3} \frac{f_{F/B}(E, T, \mu_{a'})}{2E}, \quad (32)$$

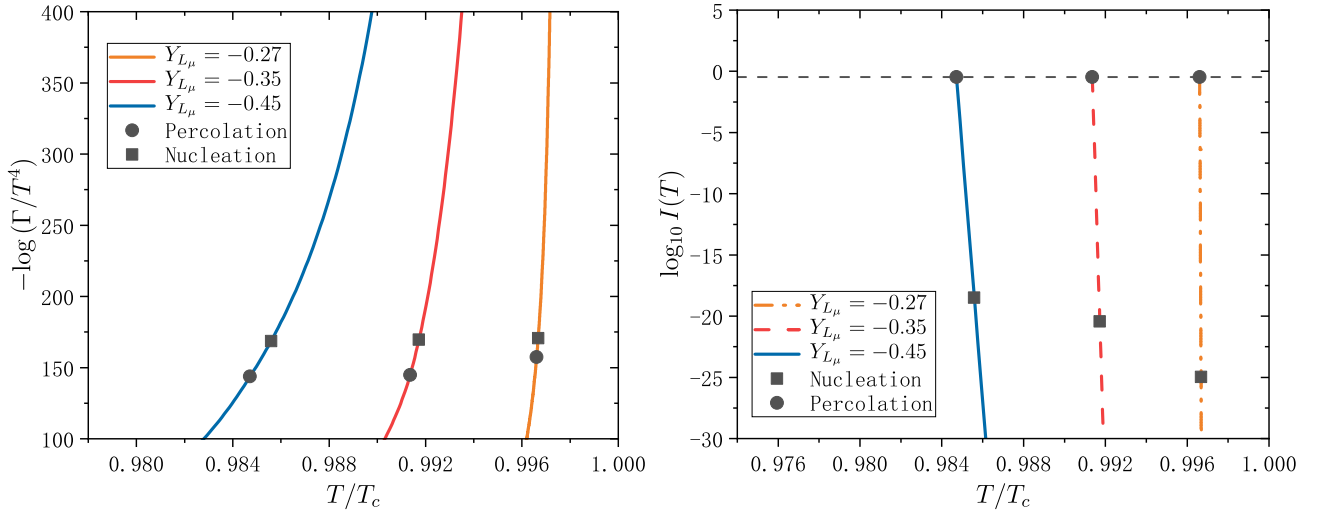


FIG. 9. The evolution of thermally-induced decay rate along the cosmic trajectory (left panel) and evolution of the false vacuum $I(T)$ along the cosmic trajectory (right panel). Black dots: percolation; Black squares: nucleation

with $\sum_{a'}$ summing over all particles taking part in the phase transition, m_f (m_t) the particle mass in false (true) vacuum and $f_{F/B}$ the Fermi–Dirac (Bose–Einstein) distribution function.

For runaway case, i.e., $\alpha > \alpha_\infty$, both bubble collisions and sound wave effects should be taken into account for the GW spectrum. The corresponding efficiency factors are:

$$\kappa_b = 1 - \frac{\alpha_\infty}{\alpha}, \quad \kappa_s = \frac{c_s^{11/5} \kappa_A \kappa_B}{(c_s^{11/5} - v_w^{11/5}) \kappa_B + v_w c_s^{6/5} \kappa_A}. \quad (33)$$

As for the non-runaway case, i.e., $\alpha < \alpha_\infty$, only the sound wave contribution should be considered. Therefore, we apply Eq. (33) and focus on the sound wave GW spectrum.

To obtain the PT parameters that take the derivative along the cosmic trajectory at finite temperature and chemical potential, we start with the fluid equation:

$$\dot{\rho}_r + 3 \frac{\dot{a}}{a} (\rho_r + p) = 0, \quad (34)$$

with

$$p = \frac{1}{3} \rho_r, \quad (35)$$

with a the scale factor, ρ_r the energy density of radiation and p the pressure. Eq. (35) is valid even for radiation in finite chemical potential. The term ρ_r considers only the radiation (except for muon due to its mass is close to the PT temperature.) because the matter energy density is much smaller than that of the radiation. The u/d quarks in the false vacuum, instead of the true vacuum, are considered in ρ_r because the decay rate $\Gamma(T, \mu)$ is that of the false vacuum. Combining Eq. (34) and Eq. (35), we obtain:

$$dt = -\frac{d\rho_r}{4H\rho_r}, \quad \rho_r = \rho_{r0} a^{-4}, \quad (36)$$

with t the time along the cosmic trajectory, $H = \frac{\dot{a}}{a}$ the Hubble parameter and ρ_{r0} the energy density at a given time. The evolution of the decay rate is calculated using the Python package `BubbleDet` [97]. In Fig. 9, the value of $-\log(\Gamma/T^4)$ is significantly influenced by the Hubble parameter that is enlarged from the energy density ρ_r .

The probability that a point still remains in the false vacuum is written as [122]:

$$P(t) = e^{-I(t)}, \quad I(t) = \frac{4\pi}{3} \int_{t_c}^t dt' \Gamma(t') a(t')^3 \left(\int_{t'}^t \frac{v_w dt''}{a(t'')} \right)^3. \quad (37)$$

After that, the formula to determine the percolation temperature and chemical potential (T_*, μ_*) can be derived by applying Eq. (36) to Eq. (37):

$$I(T, \mu) = \frac{4\pi}{3} \int_{\rho_r}^{\rho_r^c} d\rho_r' \frac{1}{4\rho_r'^{7/4}} \frac{\Gamma(T', \mu')}{H(T', \mu')} \times \left(\int_{\rho_r}^{\rho_r'} d\rho_r'' \frac{v_w}{4H(T'', \mu'') \rho_r''^{3/4}} \right)^3, \quad (38)$$

with $H = \sqrt{\frac{\rho_r + \Delta\Gamma_\Sigma}{3M_p^2}}$, and (T, μ) varying along the cosmic trajectory, H the Hubble parameter, $\rho_r = \rho_r(T, \mu)$ the energy density of the radiation, ρ_r^c the energy density when the false and the true vacuum are degenerate, and $\Delta\Gamma_\Sigma = -\Delta P$ the energy difference between false and true vacuum. The percolation temperature T_* is obtained by typically choosing $I(T_*, \mu_*) \simeq 0.34$ [122], as shown in Fig. 9. Unlike the case of vanishing chemical potential [106], the evolution of $I(T)$ is approximately linear, because its evolution primarily depends on the chemical potential.

Similarly, the inverse PT duration β/H_* can be derived with Eq. (36):

$$\beta = -\frac{d}{dt} \left(\frac{S_3}{T} \right) \Big|_{t_*} = 4H_* \rho_r \frac{d}{d\rho_r} \left(\frac{S_3}{T} \right) \Big|_{(T_*, \mu_*)}, \quad (39)$$

where the derivative lies along the cosmic trajectory.